Stability Analysis of a Turbocharger Rotor System Supported on Floating Ring Bearings

H Zhang[1,2], Z Q Shi[1,3], D Zhen[2], F S Gu[2] and A D Ball[2]
[1]Hebei University of Technology, Tianjin, 300130, P.R China
[2]University of Huddersfield, Huddersfield, HD1 3DH, UK
[3]State Key Laboratory of Mechanical Science and Vibration, Shanghai jiaotong University, Shanghai, 200240, P.R China

E-mail: a.ball@hud.ac.uk

Abstract. The stability of a turbocharger rotor is governed by the coupling of rotor dynamics and fluid dynamics because the high speed rotor system is supported on a pair of hydrodynamic floating ring bearings which comprise of inner and outer fluid films in series. In order to investigate the stability, this paper has developed a finite element model of the rotor system with consideration of such exciting forces as rotor imbalance, hydrodynamic fluid forces, lubricant feed pressure and dead weight. The dimensionless analytical expression of nonlinear oil film forces in floating ring bearings have been derived on the basis of short bearing theory. Based on numerical simulation, the effects of rotor imbalance, lubricant viscosity, lubricant feed pressure and bearing clearances on the stability of turbocharger rotor system have been studied. The disciplines of the stability of two films and dynamic performances of rotor system have been provided.

Keywords: Turbocharger, rotor system, nonlinear forces, floating ring bearing, stability analysis
Funded by State Key Laboratory of Mechanical Science and Vibration MSV-2011-22

1. Introduction

Turbochargers have been widely used in vehicles to recycle the exhaust energy and boost engine power. A typical automotive turbocharger comprises of a turbine and a compressor connected by a shared shaft supported on a floating ring bearing system. Because the working speed of a turbocharger can easily reach 140,000r/min, even a weak vibration could destroy a bearing and reduce the service life of the turbocharger. On the other hand, the turbocharger rotor is supported on a pair of hydrodynamic floating ring bearings comprised of inner and outer fluid films in series, the coupling of rotor dynamics and fluid dynamics governs the stability of a turbocharger rotor. Therefore it would be meaningful to conduct with research on the stability characteristics of a turbocharger rotor system under coupling of such multi-field forces.

As the rotor system is supported on hydrodynamic journal bearings, the nonlinear oil film force will affect dynamics performances. Many researchers have paid their attention to this issue. A. C. Hagg [1], B. Sternlicht [2] and J. W. Lund [3] firstly proposed a theory to couple oil film forces on a rotor system. Hydrodynamic fluid force in this theory is expressed by the function of displacement and

velocity around the equilibrium position and accordingly the dynamic characteristic of a journal bearing is expressed by linearized coefficients such as stiffness and damping coefficients. By solving Reynolds Equation, oil film pressure can be obtained and hydrodynamic fluid force could then be calculated by integrating oil film pressure. The situation will deteriorate if the non-linear pressure is coupled with some chaotic behaviour. Goldman et al. [4] found the chaotic behaviour of rotor/stator systems with rub-impact which may occur under certain conditions. Chu et al. [5] investigated the nonlinear vibration characteristics of a rub-impact Jeffcott. They found that when the rotating speed is increased, the grazing bifurcation, the quasi-periodic motion and chaotic motion occur after the rub-impact. Chang-Jian et al. [6-9] presented a series of papers on the nonlinear dynamics of rotor-bearing systems under nonlinear suspension and combined with rub-impact effect, turbulent effect and micropolar lubricant, they found numerous non-periodic responses occurring in the rotor-bearing systems.

Compared to the ordinary journal bearing system, a pair of floating ring bearings in a turbocharger rotor comprise of two fluid films in series. Because the inner and outer oil films affect each other, and the wide range of turbocharger working speed might cover multiple orders critical speeds, its stability analysis is much more complicated. The conventional theories based on the rigid body rotor models are no longer suited to analyze the turbocharger rotor system. Against the dynamic performance and stability of the flexible rotor system supported on the hydrodynamic floating ring bearings, researchers have proceeded with further research. Tanaka et al. [10] developed a dynamics model for flexible rotor supported on floating ring bearings based on short bearing theory and then estimated the stable speed under different bearings parameters. Through comparison between predicted and experimental results, it was demonstrated that the frequency of oil film whirl is approximately one haft of the sum of shaft speed and ring speed under medium pressure. A model for a turbocharger turbine under pulsating inlet conditions was developed by Chen et al. [11] and Kreuz-Ihli et al. [12] with experimental validation. Peat et al. [13] presented a model against the passive acoustic behaviour of turbine impeller of an automotive turbocharger. Payri et al. [14,15] published a series of papers which concentrate on the transient performance of turbocharged diesel engines and developed an action model for calculating the transient operation. On the other hand, the detection of instabilities in a turbocharger rotor system was discussed by Aretakis et al. [16] by using vibration and noise signals of the compressor impeller.

Although different aspects of stability have been investigated, the stability discipline of turbocharger rotor systems under various working conditions is still not clear so far due to the complicated nonlinear characteristics. The satisfactory analytical expression to the hydrodynamic fluid forces in floating ring bearings is also difficult to derive. Aiming at this purpose, this paper develops a mathematical model against a turbocharger rotor system supported on floating ring bearings. Following model development, bending vibration has been predicted by given parameters. According to the simulation results, dynamic performances of turbocharger rotor systems have been studied and stability disciplines have been analyzed under different working conditions.

2. Mathematical Modeling

2.1 Finite Element Model

As shown in Figure 1, a turbocharger rotor consists of turbine and compressor impellers on a shared shaft supported by a pair of floating ring bearings. The physical model and its finite element expression are shown in Figure 2(a) and (b). According to the theory of finite element method, the turbocharger rotor has been modelled as six mass nodes connected by elastic shaft segments.

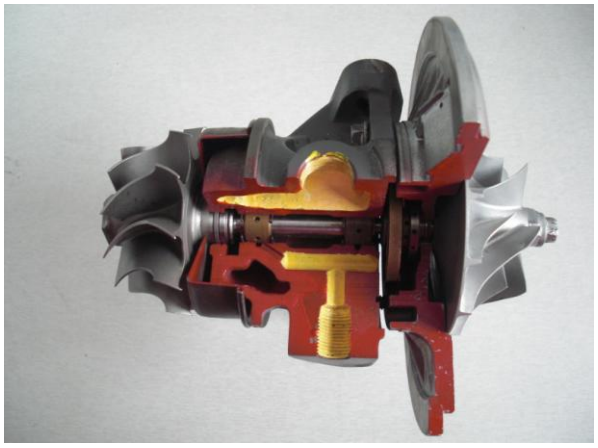

Figure 1. Turbocharger rotor system.

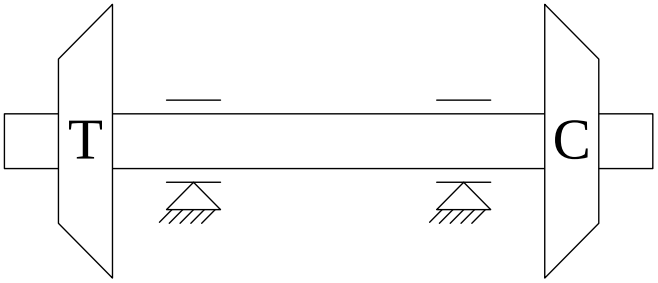

Figure 2(a). Physical model of turbocharger rotor system.

Figure 2(b). Finite element model of turbocharger rotor system.

As rotor mass is distributed on the mass nodes, a simplified mass matrix will become diagonal as in equation (1).

$$[M]=\begin{bmatrix} m_1 & & & & & \\ & m_2 & & & & \\ & & m_3 & & & \\ & & & m_4 & & \\ & & & & m_5 & \\ & & & & & m_6 \end{bmatrix} \tag{1}$$

Assume the materials of turbocharger shaft to be uniformed and then stiffness and damping matrices of rotor system can be expressed as follows:

$$[K]=\begin{bmatrix} k_1 & -k_1 & & & & \\ -k_1 & k_1+k_2 & -k_2 & & & \\ & -k_2 & k_2+k_3 & -k_3 & & \\ & & -k_3 & k_3+k_4 & -k_4 & \\ & & & -k_4 & k_4+k_5 & -k_5 \\ & & & & -k_5 & k_5 \end{bmatrix} \tag{2}$$

$$[C]=\begin{bmatrix} c_1 & -c_1 & & & & \\ -c_1 & c_1+c_2 & -c_2 & & & \\ & -c_2 & c_2+c_3 & -c_3 & & \\ & & -c_3 & c_3+c_4 & -c_4 & \\ & & & -c_4 & c_4+c_5 & -c_5 \\ & & & & -c_5 & c_5 \end{bmatrix} \tag{3}$$

Major exciting forces for turbocharger rotor system bending vibration include static and dynamic loads. Static loads denote such constant loads as lubricant feed pressure, dead weights of rotor, etc. Dynamic loads denote such variable forces as hydrodynamic fluid forces, rotor imbalance centrifugal forces, etc. After forming the system mass, stiffness and damping matrices, the motion equation of turbocharger shaft is expressed in equation (4).

$$[M]\{\ddot{U}\}+[C]\{\dot{U}\}+[K]\{U\}=\{W\}+\{F_u\}+\{Fh_{inner}\} \tag{4}$$

where $\{U\}=\{x_1,...,x_6,y_1,...,y_6\}$ represent displacements of the nodes in horizontal and vertical direction, i.e. X and Y direction. $[M],[C],[K]$ represent mass, damping and stiffness matrices respectively. On the right hand side of the equation, major exciting forces include imbalance centrifugal forces $\{F_u\}$, hydrodynamic fluid force in inner oil film $\{Fh_{inner}\}$ and the dead weight $\{W\}$.

Motion of the floating ring is determined by the hydrodynamic fluid forces of inner and outer films, lubricant feed pressure and dead weight of the ring. The motion equation is given by equation (5).

$$[M_R]\{\ddot{U}_R\}=\{Fh_{outer}\}-\{Fh_{inner}\}+\{W_R\}+\{P\} \tag{5}$$

where U_R represents the displacements of the floating ring, M_R is mass matrix of the ring. Exciting force vectors include hydrodynamic forces of two oil films, lubricant feed pressure and the dead weight of the ring.

Since the shaft and the floating ring influence each other, the motion of them should be solved simultaneously. Thus couple equation (4) and (5) to form the motion equation of the rotor system (6).

$$\begin{bmatrix}[M] & [0]\\ [0] & [M_R]\end{bmatrix}\begin{Bmatrix}\ddot{U}\\ \ddot{U}_R\end{Bmatrix}+\begin{bmatrix}[C] & [0]\\ [0] & [0]\end{bmatrix}\begin{Bmatrix}\dot{U}\\ \dot{U}_R\end{Bmatrix}+\begin{bmatrix}[K] & [0]\\ [0] & [0]\end{bmatrix}\begin{Bmatrix}U\\ U_R\end{Bmatrix}=\{F\}$$

$$\{F\}=\begin{Bmatrix}F_u\\ 0\end{Bmatrix}+\begin{Bmatrix}W\\ W_R\end{Bmatrix}+\begin{Bmatrix}0\\ P\end{Bmatrix}+\begin{Bmatrix}Fh_{inner}\\ Fh_{outer}-Fh_{inner}\end{Bmatrix} \tag{6}$$

2.2 Hydrodynamic Fluid Force

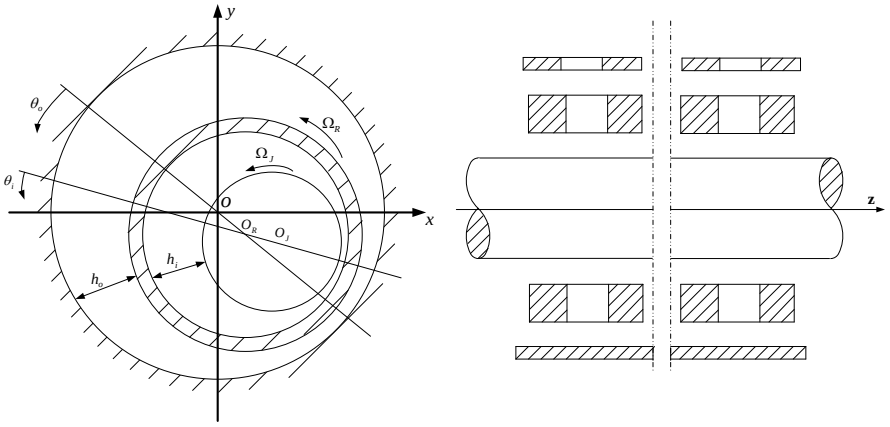

Figure 3. Coordinate system of the floating ring bearing.

Figure 3 shows the coordinate system of the floating ring bearing, hydrodynamic fluid forces can be derived from the film pressure distribution. Dimensionless Reynolds equation for outer fluid film is expressed by

$$\frac{\partial}{\partial\theta}\left(h_o^3\frac{\partial p_o}{\partial\theta}\right)+\left(\frac{R_o}{L}\right)^2\frac{\partial}{\partial z}\left(h_o^3\frac{\partial p_o}{\partial z}\right)=\frac{\partial h_o}{\partial\theta}+2\frac{\partial h_o}{\partial\tau_o} \tag{7}$$

where h_o is the thickness of outer film, C_o is the outer clearance, R_o is the radius of outer ring, L is bearing length.

Assume that lubricant is incompressible and viscosity is constant during simulation, after ignoring the pressure gradient in the circumferential direction and applying short bearing theory to deal with the dimensionless Reynolds equations. Theoretical solutions of the differential equation for outer fluid films is given by

$$p_o=\frac{1}{2}\left(\frac{L}{D_o}\right)^2\left[\frac{(x_R-2\dot{y}_R)\sin\theta-(y_R+2\dot{x}_R)\cos\theta}{(1-x_R\cos\theta-y_R\sin\theta)^3}\right](4z^2-1) \tag{8}$$

Integrating oil film pressure in the outer oil film field, hydrodynamic fluid forces of outer film are expressed as follows.

$$\begin{Bmatrix}Fh_{outer\_x}\\Fh_{outer\_y}\end{Bmatrix}=-\mu\Omega_R\left(\frac{R_o^2}{C_o^2}\right)\left(\frac{L^2}{D_o^2}\right)(R_oL)\frac{\sqrt{(x_R-2\dot{y}_R)+(y_R+2\dot{x}_R)}}{(1-x_R\cos\theta-y_R\sin\theta)}$$

$$\begin{Bmatrix}3x_RV_o-\sin\alpha_oG_o-2\cos\alpha_oF_o\\3y_RV_o-\cos\alpha_oG_o-2\sin\alpha_oF_o\end{Bmatrix}$$

$$V_o=\frac{2+(y_R\cos\alpha_o-x_R\sin\alpha_o)G_o}{(1-x_R^2-y_R^2)}$$

$$G_o=\frac{\pi}{\sqrt{1-x_R^2-y_R^2}}-\frac{2}{\sqrt{1-x_R^2-y_R^2}}\tan^{-1}\left(\frac{y_R\cos\alpha_o-x_R\sin\alpha_o}{\sqrt{1-x_R^2-y_R^2}}\right)$$

$$F_o=\frac{(x_R\cos\alpha_o+y_R\sin\alpha_o)}{(1-x_R^2-y_R^2)}$$

$$\alpha_o=\tan^{-1}\left(\frac{y_R+2\dot{x}_R}{x_R-\dot{y}_R}\right)-\frac{\pi}{2}sign\left(\frac{y_R+2\dot{x}_R}{x_R-\dot{y}_R}\right)-\frac{\pi}{2}sign(y_R+2\dot{x}_R) \tag{9}$$

Dimensionless Reynolds equation for inner film is expressed by

$$\frac{\partial}{\partial\theta}\left(h_i^3\frac{\partial p_i}{\partial\theta}\right)+\left(\frac{R_J}{L}\right)^2\frac{\partial}{\partial z}\left(h_i^3\frac{\partial p_i}{\partial z}\right)=\frac{\partial h_i}{\partial\theta}+2\frac{\partial h_i}{\partial\tau_i} \tag{10}$$

Integrating inner film pressure in the inner oil film field, hydrodynamic forces could be expressed as follows.

$$\begin{Bmatrix}Fh_{inner\_x}\\Fh_{inner\_y}\end{Bmatrix}=-\mu\left(\Omega_J+\frac{R_i}{R_J}\Omega_R\right)\left(\frac{R_J^2}{C_i^2}\right)\left(\frac{L^2}{D_i^2}\right)(R_J L)\frac{\sqrt{(x_i-2\dot{y}_i)+(y_i+2\dot{x}_i)}}{(1-x_i\cos\theta-y_i\sin\theta)}$$

$$\begin{Bmatrix}3x_iV_i-\sin\alpha_iG_i-2\cos\alpha_iF_i\\3y_iV_i-\cos\alpha_iG_i-2\sin\alpha_iF_i\end{Bmatrix}$$

$$V_i=\frac{2+(y_i\cos\alpha_i-x_i\sin\alpha_i)G_i}{(1-x_i^2-y_i^2)}$$

$$G_i=\frac{\pi}{\sqrt{1-x_i^2-y_i^2}}-\frac{2}{\sqrt{1-x_i^2-y_i^2}}\tan^{-1}\left(\frac{y_i\cos\alpha_i-x_i\sin\alpha_i}{\sqrt{1-x_i^2-y_i^2}}\right)$$

$$F_i=\frac{(x_i\cos\alpha_i+y_i\sin\alpha_i)}{(1-x_i^2-y_i^2)}$$

$$\alpha_i=\tan^{-1}\left(\frac{y_i+2\dot{x}_i}{x_i-\dot{y}_i}\right)-\frac{\pi}{2}sign\left(\frac{y_i+2\dot{x}_i}{x_i-\dot{y}_i}\right)-\frac{\pi}{2}sign(y_i+2\dot{x}_i) \tag{11}$$

It can be seen that hydrodynamic forces of inner and outer oil films are calculated based on different normalization standard Reynolds equation, so that the results could not be calculated with each other directly. It is necessary to unify the normalization standard. In this paper, normalization standard has been chosen on the basis of outer oil film. Parameters of relative displacement between journal and floating ring are given by

$$x_i=(x-x_R)\frac{C_o}{C_i},\ y_i=(y-y_R)\frac{C_o}{C_i},\ h_i=1-(x-x_R)\frac{C_o}{C_i}\cos\theta-(y-y_R)\frac{C_o}{C_i}\sin\theta$$

$$\dot{x}_i=(\dot{x}-\dot{x}_R)\frac{\Omega_R}{\left(\Omega_J+\frac{R_i}{R_J}\Omega_R\right)},\ \dot{y}=(\dot{y}-\dot{y}_R)\frac{\Omega_R}{\left(\Omega_J+\frac{R_i}{R_J}\Omega_R\right)}$$

Following hydrodynamic fluid forces calculation, these forces will be converted into the standard of fluid force in outer film by multiplying a coefficient $\left(\frac{\Omega_J}{\Omega_R}+\frac{R_i}{R_J}\right)\frac{R_J^2C_o^2}{R_o^2C_i^2}$

The rotational speed of the floating ring is estimated by equation (12) in which the speed ratio between floating ring and journal is considered as constant.

$$\frac{\Omega_R}{\Omega_J}=\frac{1}{1+R_o^3/R_i^3\cdot C_i/C_o} \tag{12}$$

Substitute hydrodynamic fluid forces of two films into system motion equation (6), numerical approach is applied to predict turbocharger rotor system bending vibration as well as the floating ring.

3. Stability Analysis

As the turbocharger is working, the shear-driven torques of two fluid films drive the floating ring spin at a certain speed that is lower than the shaft speed. The outer oil film is formed by the rotating ring and bearing shell. When the floating ring reaches a certain speed, the outer film will become unstable and rotor would theoretically be whirling at the angular frequency of less than half of ring speed. The inner oil film is formed by the shaft and floating ring. According to the theory of Hydrodynamic

Lubrication, oil film between two rotating surfaces can be viewed as the film between a static surface and a rotating surface which spins at the sum rotational speed. As the rotational speed reaches a certain speed, the inner oil film becomes unstable and the rotor would theoretically be whirling at the angular frequency of less than half of the sum speed of the journal and floating ring.

Stability of the whole rotor system depends upon two such interdependent oil films. In the following sections, the affects of rotor imbalance, lubricant viscosity, and lubricant feed pressure and bearing clearances on the stability of a turbocharger rotor system have been studied according to the simulation results from the theoretical model.

3.1. Influences of Rotor Imbalance

Rotor imbalance is an inevitable fault in all rotor systems. The centrifugal forces caused by rotor imbalance could excite the synchronous motion when angular frequency is approximately the same as shaft speed. In addition, rotor imbalance could also affect the stability of rotor system. Table 1 lists simulation parameters in rotor imbalance analysis.

Table 1. Simulation parameters in rotor imbalance analysis.

Parameters	Values
Lubricant viscosity	12cp
Outer radius of the ring	$9\times10^{-3}m$
Inner radius of the ring	$5\times10^{-3}m$
Outer clearance of the bearing	$8\times10^{-5}m$
Inner clearance of the bearing	$2\times10^{-5}m$
Static load on floating ring	0

In order to simulate the rotor imbalance, relative eccentricity is assumed to be exerted on the turbine mass node. The motions of the turbocharger shaft end on the turbine impeller side are displayed. Normalized angular frequency denotes the frequency ratio between the shaft motion and its rotational speed.

Figure 4 illustrates waterfall and bifurcation diagrams of turbocharger shaft end motion within 15,000rad/s under 0.2, 0.3 and 0.4 relative eccentricities. It is clear that synchronous component exists in all three cases within the whole speed range due to the assumed rotor imbalance. Under a small imbalance, the rotor system performs synchronous motion only at low rotational speed. As the shaft speed increases, inner oil film initially becomes unstable which excites the sub-synchronous component of approximately 40% of shaft speed. If the shaft speed increases even further, instability occurs in the outer oil film and dominates the motion of rotor system within a wide speed range. Under a larger imbalance, inner film enters into instable at a relative lower speed. However such instability will shortly disappear and the rotor system become stable again. Synchronous component dominates system motion until a high speed is reached, when instability will appear in turn in the inner and outer films which angular frequencies are approximately 40% and 18% of shaft speed respectively. It can be deduced that the centrifugal forces caused by rotor imbalance could inhibit the appearance of instability in a degree that makes the rotor system keep stable within a wide speed range. On the other hand, rotor imbalance will not affect the sequence of instabilities appearing in two films.

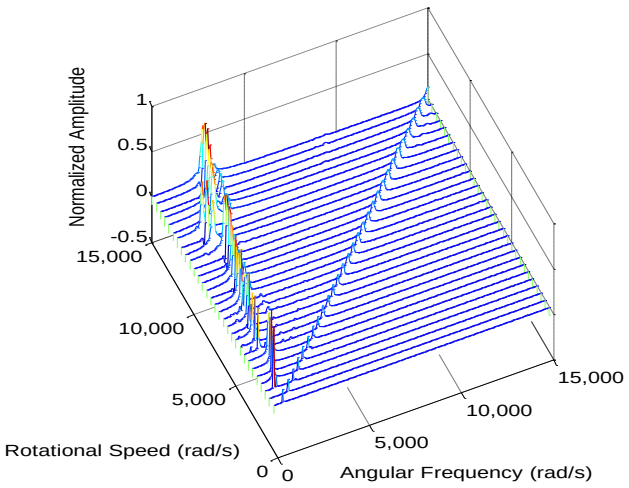
Normalized Amplitude
1
0.5
0
-0.5
15,000
10,000
5,000
0
Rotational Speed (rad/s)
0
5,000
10,000
15,000
Angular Frequency (rad/s)

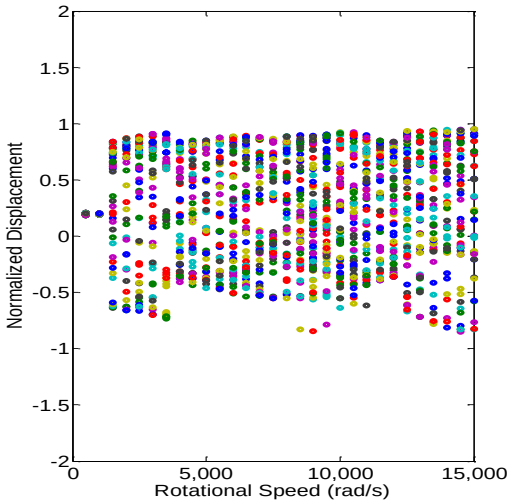
Normalized Displacement
2
1.5
1
0.5
0
-0.5
-1
-1.5
-2
0
5,000
10,000
15,000
Rotational Speed (rad/s)

(a)

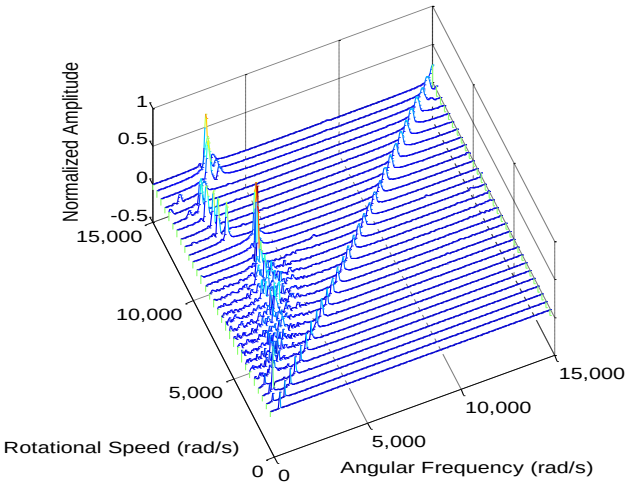
Normalized Amplitude
1
0.5
0
-0.5
15,000
10,000
5,000
0
Rotational Speed (rad/s)
0
5,000
10,000
15,000
Angular Frequency (rad/s)

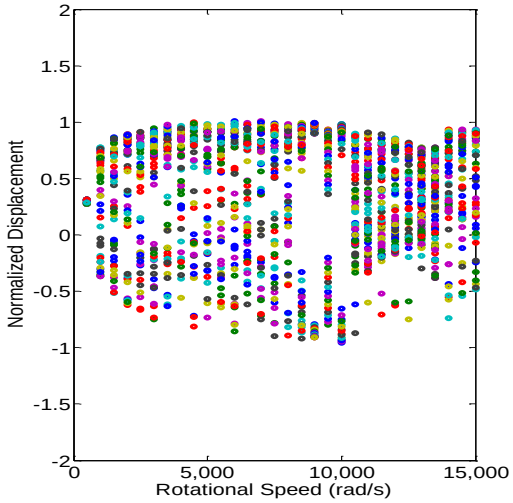
Normalized Displacement
2
1.5
1
0.5
0
-0.5
-1
-1.5
-2
0
5,000
10,000
15,000
Rotational Speed (rad/s)

(b)

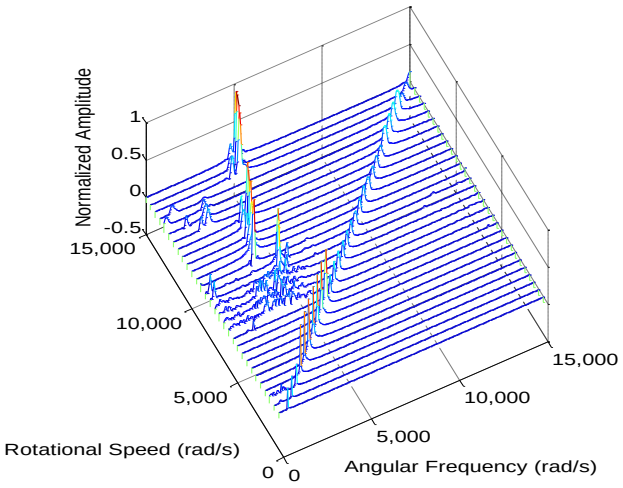
Normalized Amplitude
1
0.5
0
-0.5
15,000
10,000
5,000
0
Rotational Speed (rad/s)
0
5,000
10,000
15,000
Angular Frequency (rad/s)

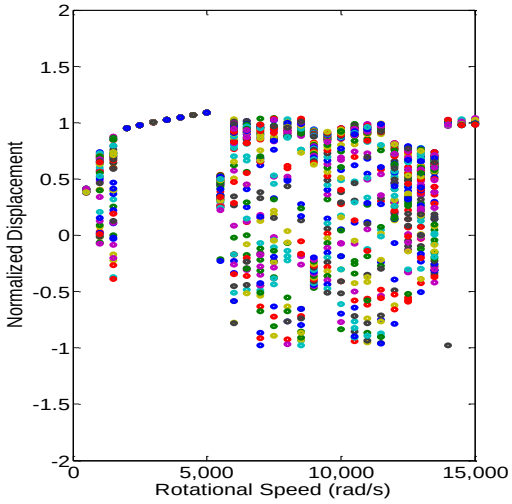
Normalized Displacement
2
1.5
1
0.5
0
-0.5
-1
-1.5
-2
0
5,000
10,000
15,000
Rotational Speed (rad/s)

(c)

Figure 4. Waterfall and bifurcation diagrams of turbocharger shaft end motion within 15,000rad/s: (a)with 0.2 relative eccentricity (b)with 0.3 relative eccentricity (c)with 0.4 eccentricity.

3.2. Influences of Lubricant Viscosity

Different lubricant viscosity leads to the change of characteristics of lubricant flow in the bearing clearances which would cause different oil film pressure distribution and hydrodynamic fluid forces around the shaft and the floating ring. Therefore the stability of the turbocharger rotor system will be influenced. Table 2 lists the simulation parameters in lubricant viscosity analysis.

Table 2. Simulation parameters in lubricant viscosity analysis.

Parameters	Values
Outer radius of the ring	$9\times10^{-3}m$
Inner radius of the ring	$5\times10^{-3}m$
Outer clearance of the bearing	$8\times10^{-5}m$
Inner clearance of the bearing	$2\times10^{-5}m$
Eccentricity on turbine node	0.2
Static load on floating ring	0

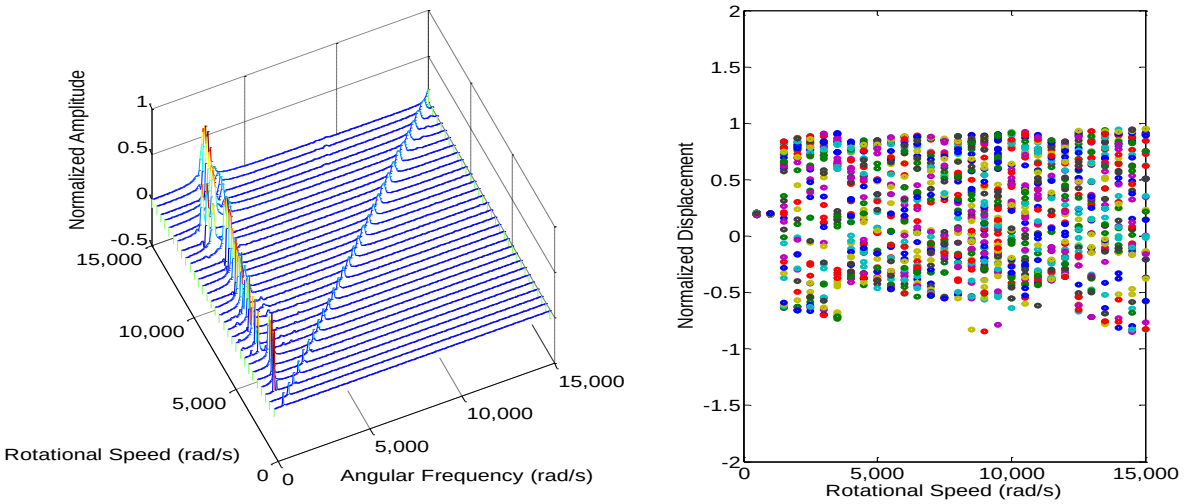

(a)

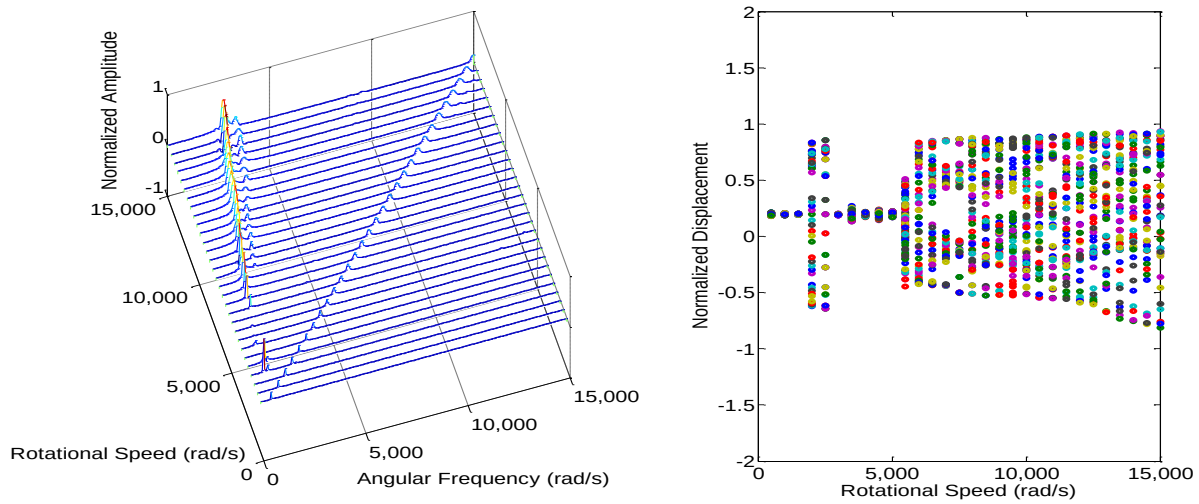

(b)

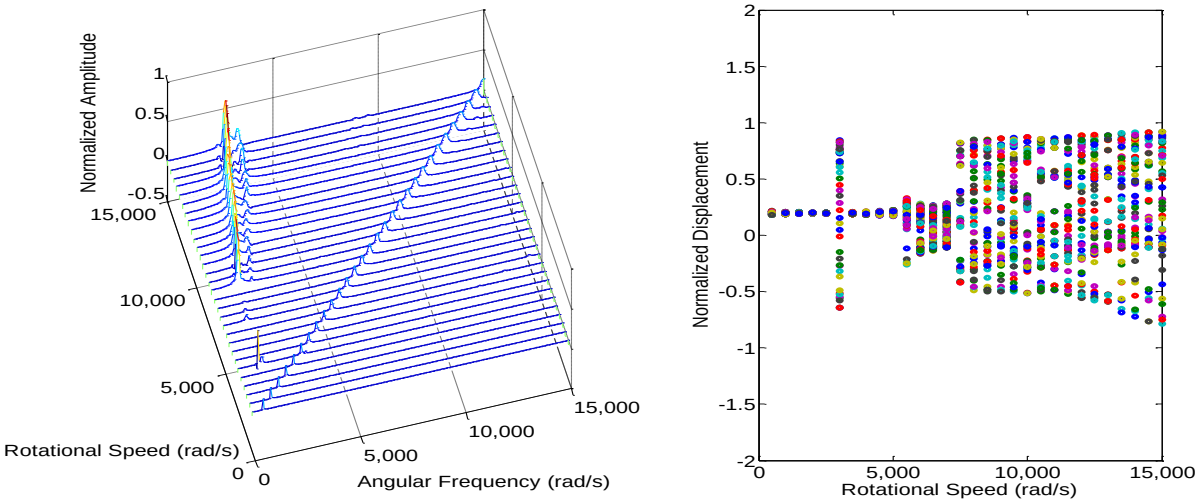

(c)

Figure 5. Waterfall and bifurcation diagrams of turbocharger shaft end motion within 15,000rad/s: (a)under 15cp lubricant viscosity (b)under 30cp lubricant viscosity (c)under 50cp lubricant viscosity.

Figure 5 illustrates waterfall and bifurcation diagrams of turbocharger shaft end motion within 15,000rad/s. It can be seen from Figure 5(b) that under 30cp lubricant viscosity, instability of the rotor system does not occur until 2,000rad/s. From 2,000 to 2,500rad/s rotational speed, oil whirl occurs in the inner film which excites the subsynchronous component of angular frequency of approximately 40% of shaft speed. Increasing the shaft speed further, inner film instability disappears and the rotor system becomes stable again. When shaft speed exceeds 5,500rad/s, the outer film becomes unstable which excites the subsynchronous component of angular frequency of approximate 18% of shaft speed. A similar stability discipline is shown in Figure 5(c). Under 50cp lubricant viscosity, the turbocharger rotor system is stable below 5,500rad/s that shows synchronous component only, except for 3,000rad/s when approximately 40% of shaft speed subsynchronous component dominate the shaft motion. It can be concluded that high lubricant viscosity could effectively inhibit the appearance of inner oil film instability that keeps the rotor system motion stable within a wide speed range before the appearance of outer film instability. On the other hand, the sequence of two films instability is not affected by lubricant viscosity.

3.3. Influences of Lubricant Feed Pressure

As far as the lubrication of floating ring bearings, lubricant is supplied into the outer film through a hole on the top of the bearing shell. The feed pressure can be simulated by static load acting on the floating ring. Table 3 lists simulation parameters in lubricant feed pressure analysis.

Table 3. Simulation parameters in lubricant feed pressure analysis.

Parameters	Values
Lubricant viscosity	15cp
Outer radius of the ring	$9\times10^{-3}m$
Inner radius of the ring	$5\times10^{-3}m$
Outer clearance of the bearing	$8\times10^{-5}m$
Inner clearance of the bearing	$2\times10^{-5}m$
Eccentricity on turbine mass node	0.2

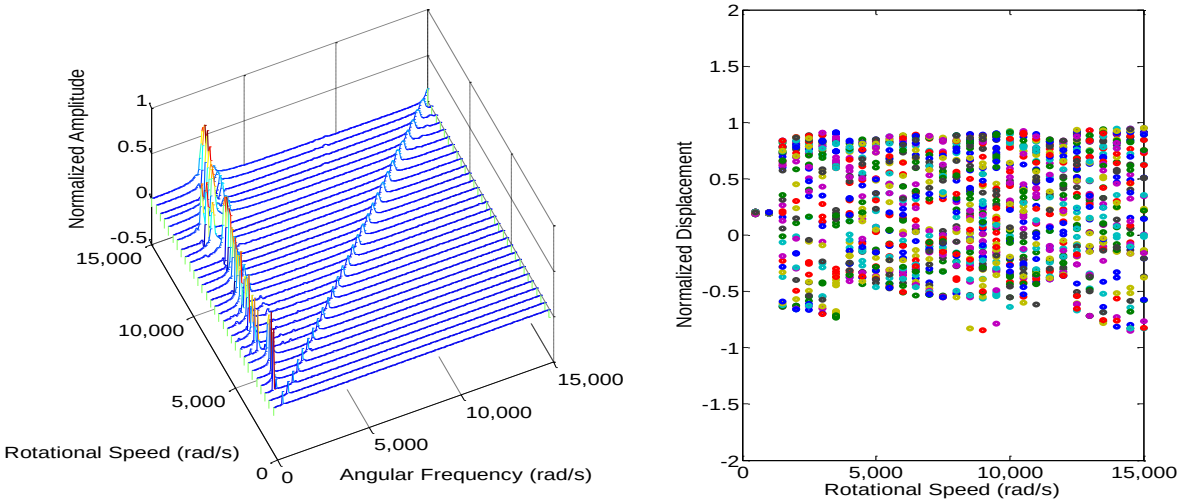

(a)

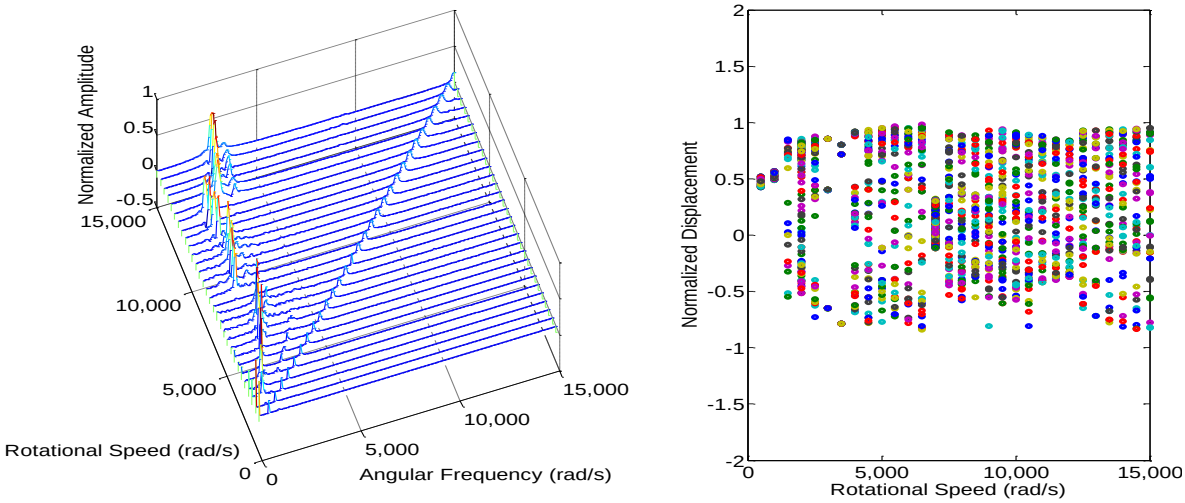

(b)

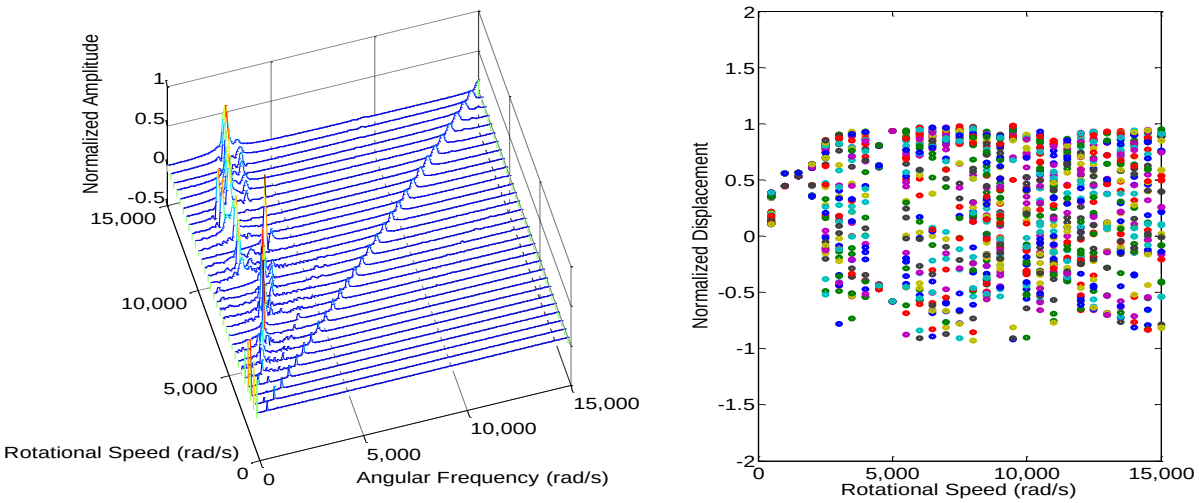

(c)

Figure 6. Waterfall and bifurcation diagrams of turbocharger shaft end motion within 15,000rad/s: (a)nil static load (b)2N static load (c)5N static load.

Figure 6 illustrate waterfall and bifurcation diagrams of turbocharger shaft end motion within 15,000rad/s rotational speed under nil, 2N and 5N static loads. Lubricant feed pressure could increase damping effects of the outer oil film that lead to inner oil film instability appear at higher speed. Oil whirl phenomenon in the outer film is also delayed. On the other hand, lubricant feed pressure might affect the sequence of two oil film instabilities. As shown in Figure 6(c), within a certain speed range, instabilities phenomena might appear in inner and outer film alternatively or simultaneously.

3.4. Influences of Bearing Clearances

Due to the extreme working condition, wear is a common fault for turbocharger hydrodynamic bearings. Due to dry friction during start-up and rub-impact phenomenon under high load et al, bearing clearances might be changed after long term usage. In this section, effects of inner and outer bearing clearances on the stability of the turbocharger rotor system are studied respectively. Table 4 lists simulation parameters in bearing clearances analysis.

Table 4. Simulation parameters in bearing clearances analysis.

Parameters	Values
Lubricant viscosity	15cp
Outer radius of the ring	$9\times10^{-3}m$
Inner radius of the ring	$5\times10^{-3}m$
Outer clearance of the bearing	$8\times10^{-5}m$; $9\times10^{-5}m$; $1\times10^{-4}m$
Inner clearance of the bearing	$2\times10^{-5}m$; $3\times10^{-5}m$; $4\times10^{-5}m$
Eccentricity on turbine mass node	0.2
Static load on floating ring	0

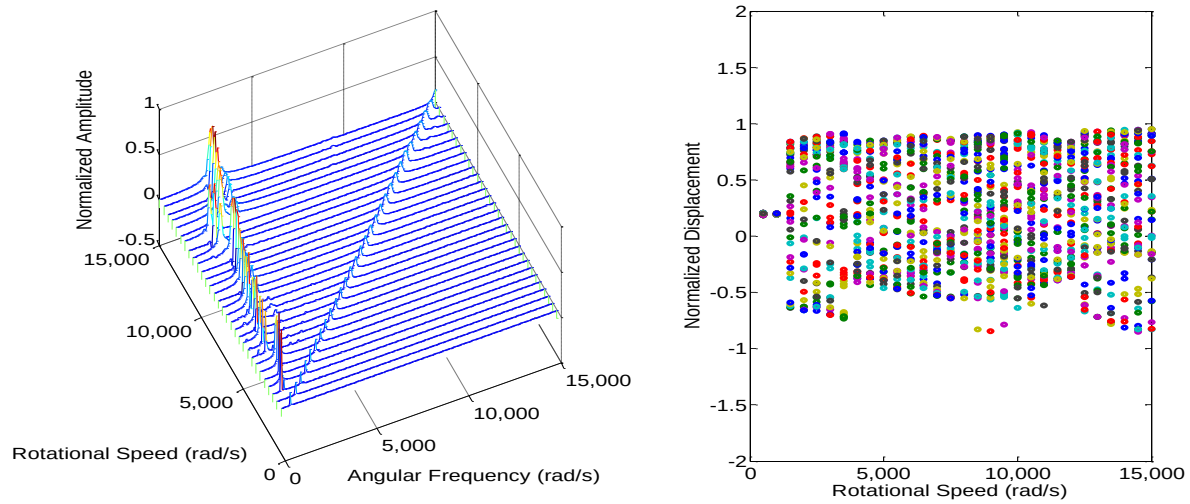
Normalized Amplitude
1
0.5
0
-0.5
15,000
10,000
5,000
0
Rotational Speed (rad/s)
0
5,000
10,000
15,000
Angular Frequency (rad/s)
Normalized Displacement
2
1.5
1
0.5
0
-0.5
-1
-1.5
-2
0
5,000
10,000
15,000
Rotational Speed (rad/s)

(a)

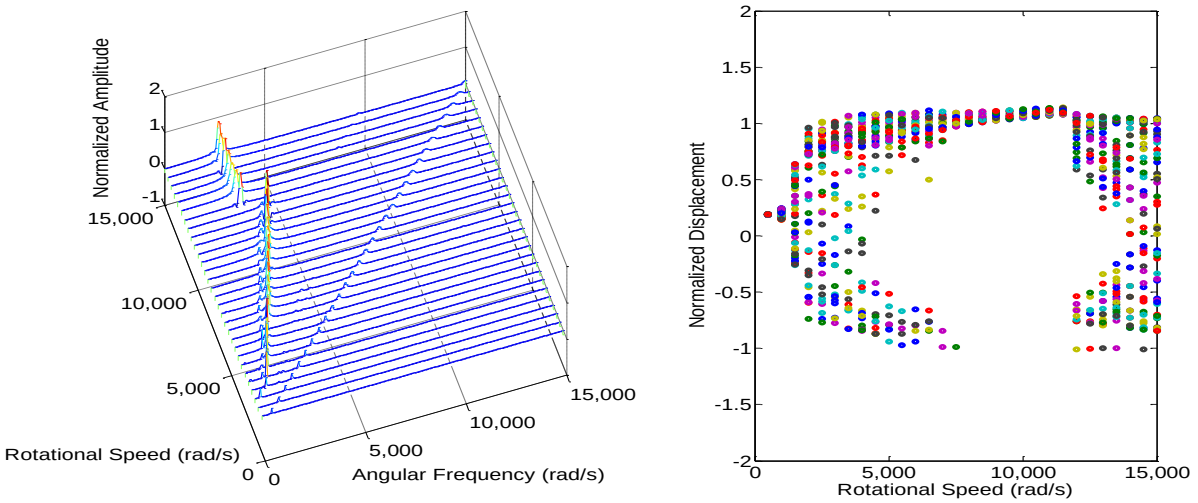
Normalized Amplitude
2
1
0
-1
15,000
10,000
5,000
0
Rotational Speed (rad/s)
0
5,000
10,000
15,000
Angular Frequency (rad/s)
Normalized Displacement
2
1.5
1
0.5
0
-0.5
-1
-1.5
-2
0
5,000
10,000
15,000
Rotational Speed (rad/s)

(b)

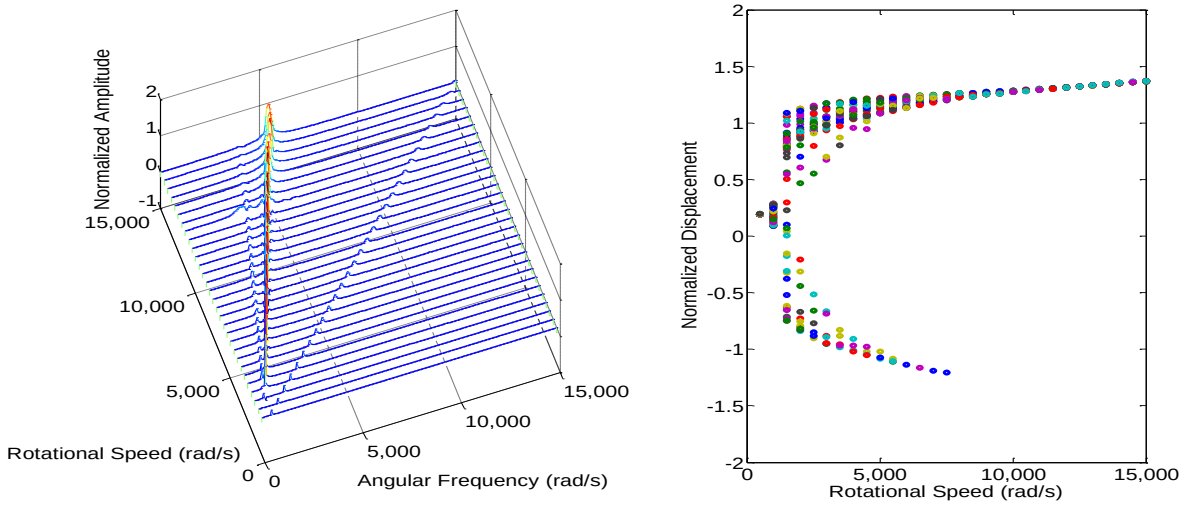

(c)

Figure 7. Waterfall and bifurcation diagrams of turbocharger shaft end motion within 15,000rad/s: (a)with $20\mu m$ inner clearance (b)with $30\mu m$ inner clearance (c)with $40\mu m$ inner clearance.

Figure 7 show the waterfall and bifurcation diagrams of turbocharger shaft end motion within 15,000rad/s rotational speed with $20\mu m$, $30\mu m$ and $40\mu m$ inner bearing clearances. In the case of $20\mu m$ inner clearance, instability is initially occurs in the inner film at 1,500rad/s rotational speed which is then replaced by outer film instability at 4,000rad/s. In the case of $30\mu m$ inner clearance, inner oil film instability occurs at 1,500rad/s and lasts until 11,000rad/s, above which speed outer film instability appears. In the case of $40\mu m$ inner clearance, within the whole speed range above 1,500rad/s, the rotor system motion is dominated by inner film instability which does not appear in the outer film. It is clear that thick inner clearance could extend the speed range of inner oil film instability. Wear occuring in inner clearance can be viewed as inner oil film area increased, which means more lubricant could be supplied into inner clearance neglecting the influence of starved lubrication. Thus damping effect is increased which inhibits effectively the outer film instability. On the other hand, inner clearance does not affect the appearance of inner oil film instability.

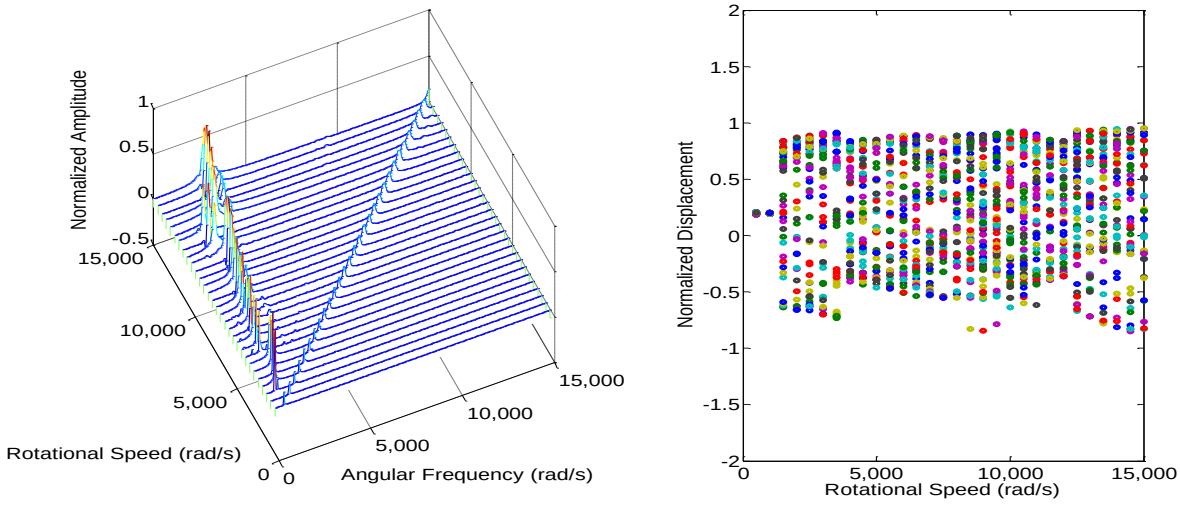

(a)

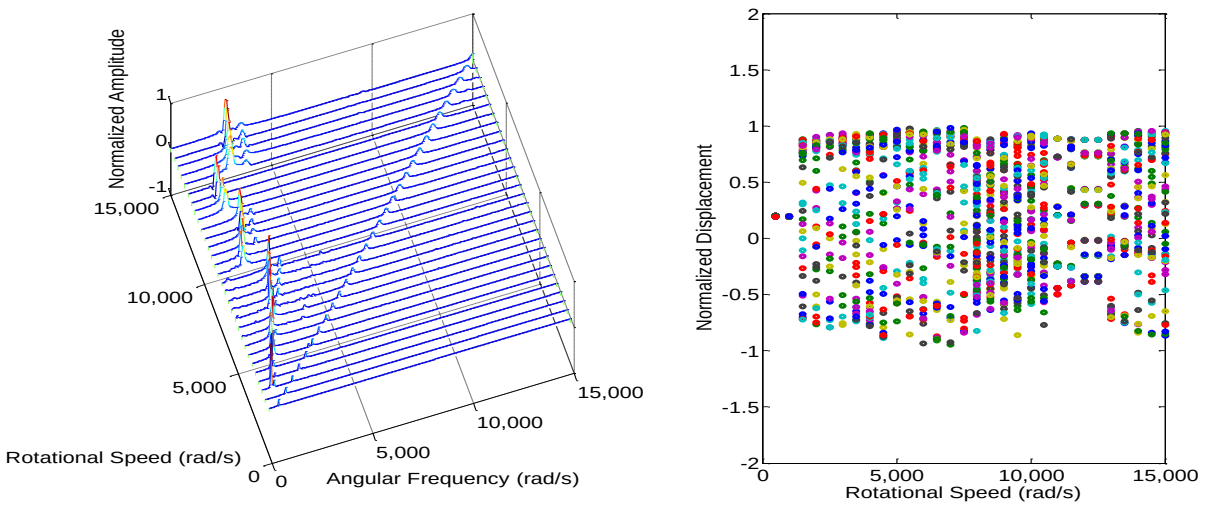

(b)

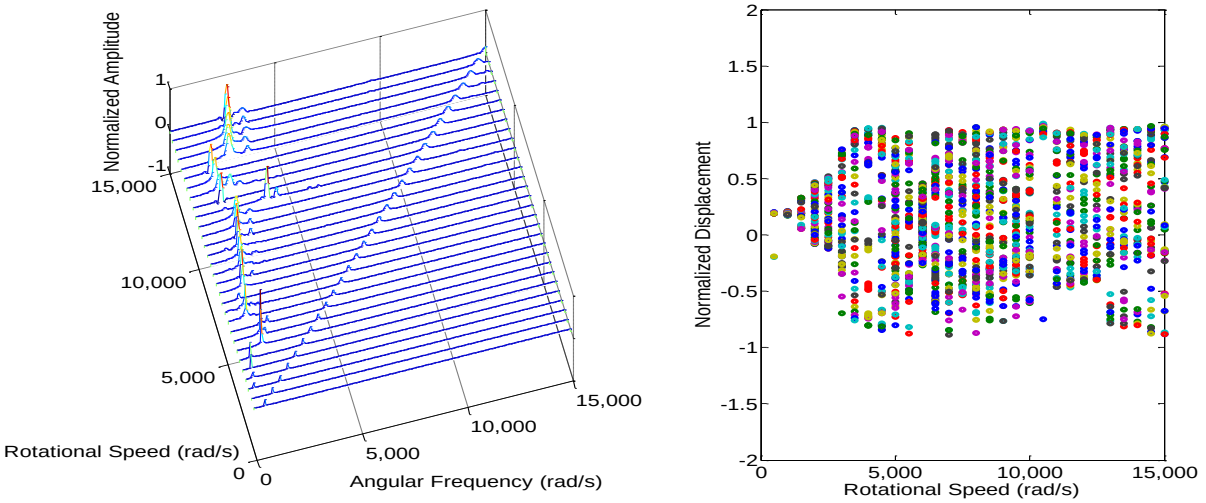

(c)

Figure 8. Waterfall and bifurcation diagrams of turbocharger shaft end motion within 15,000rad/s: (a)with $80\mu m$ outer clearance (b)with $90\mu m$ outer clearance (c)with $100\mu m$ outer clearance.

Figure 8 illustrates waterfall and bifurcation diagrams of turbocharger shaft end motion within 15,000rad/s rotational speed with $80\mu m$, $90\mu m$ and $100\mu m$ outer clearances. It can be seen that the rotor system shows stable motion below 1,000rad/s in the case of $90\mu m$ outer bearing clearance and then the sub-synchronous component of approximately 40% of shaft speed. When shaft speed exceeds 8000rad/s, the sub-synchronous component of approximately 18% of shaft speed dominates the rotor system motion. In the case of $100\mu m$ outer bearing clearance, the sub-synchronous component of approximately 18% of shaft speed initially occurred at 1,500rad/s. Between 3,500rad/s and 4,500rad/s it is replaced by the sub-synchronous component of approximate 40% of shaft speed. When exceeding 5,000rad/s, system motion is dominated by the 18% of shaft speed sub-synchronous component again. It can be deduced that outer clearance might lead to the change of the sequence of the oil film instabilities. The outer film might enter into instability initially under large outer clearance.

4. Conclusion

In this paper, a finite element model is developed for the turbocharger rotor system considering the coupling of rotor imbalance, hydrodynamic fluid forces, lubricant feed pressure and the dead weight. The dimensionless analytical expression of nonlinear oil film forces have been derived based on the short bearing theory. The coupled rotor system motion equation is solved by MATLAB software to predict bending vibration of the shaft and floating ring.

Theoretical simulation results are used to analyse the effects of rotor imbalance, lubricant viscosity, lubricant feed pressure and bearing clearances on the stability of turbocharger rotor system. It is found that there are mainly three vibration components appearing within a normal working speed range of the turbocharger. They are synchronous component when angular frequency is the same as shaft speed, sub-synchronous component when angular frequency is approximately 40% of shaft speed, sub-synchronous component when angular frequency is approximately 18% of shaft speed, which are caused by rotor imbalance, inner oil film instability and outer oil film instability respectively.

As far as rotor system stability is concerned, rotor imbalance and high lubricant viscosity could inhibit the appearance of instability in a degree that makes the rotor system remain stable within a wide speed range. Lubricant feed pressure, as a static load exerted on the floating ring, could increase damping affects of outer oil film that leads to inner oil film instability appearing at higher speed. Oil whirl phenomenon in the outer film would also be delayed. Bearing wear in inner clearance can be viewed as inner oil film area increased, which means more lubricant could be supplied into inner clearance. Thus damping effect is increased which then inhibits effectively the outer film instability. Outer bearing clearance could lead to the change of the sequence of oil film instabilities.

References

[1] Hagg AC 1956 Some dynamic properties of oil film journal bearings. *Trans. ASME, J. Eng*. **3** 302-306

[2] Sternlicht B 1959 Elastic and damping properties of cylindrical journal bearings. *J. Basic Eng*. **81** 101-108

[3] Lund JW 1964 Spring and damping coefficients for the tilting pad journal bearing. *Trans. ASLE* **7** 342-352

[4] Goldman P and Muszynska A 1994 Chaotic behavior of rotor/stator systems with rubs. *Trans. ASME, J. Eng. Gas Turbines Power* **116** 692-701

[5] Chu F and Zhang Z 1998 Bifurcation and chaos in rub-impact jeffcott rotor system. *J. Sound Vib.* **210** 1-18

[6] Chang-Jian CW and Chen CK 2006 Bifurcation and chaos of a flexible rotor supported by turbulent journal bearings with non-linear suspension. *Trans. IMechE, Part J: J. Eng. Tribol*. **220** 549-561

[7] Chang-Jian CW and Chen CK 2006 Nonlinear dynamic analysis of a flexible rotor supported by micropolar fluid film journal bearings. *Int J. Eng. Sci*. **44** 1050-1070

[8] Chang-Jian CW and Chen CK 2007 Chaos and bifurcation of a flexible rub-impact rotor supported by oil film bearings with non-linear suspension. *Mech. Mach. Theory* **42** 312-333

[9] Chang-Jian CW and Chen CK 2007 Bifurcation and chaos analysis of a flexible rotor supported by turbulent long journal bearings. *Chaos, Solitons Fractals* **34** 1160-1179

[10] Tanaka M and Hori Y 1972 Stability characteristics of floating bush bearings. *Trans. ASME, J. Lubr. Technol*. **94** 248-259

[11] Chen H, Hakeem I and Martinez-Botas RF 1996 Modelling of a turbocharger turbine under pulsating inlet conditions. *IMchE, Part A: J. Power Energy* **210** 397-408

[12] Kreuz-Ihli T, Filsinger D, Shulz A, et al 2000 Numerical and experimental study of unsteady flow field and vibration in radial inflow turbines. *J. Turbomach*. **122** 247-254

[13] Peat KS, Torregrosa AJ, Broatch A, et al 2006 An investigation into the passive acoustic effect of the turbine in an automotive turbocharger. *J. Sound Vib*. **295** 60-75

[14] Payri F, Benajes J and Reyes M 1995 Modelling of a supercharger turbines in internal-combustion diesel engines. *Int. J. Mech. Sci*. **38** 853-869
[15] Payri F, Desantes JM, Broatch A 2000 Modified impulse method for the measurement of the frequency response of acoustic filters to weakly nonlinear transient excitations. *J. Acoust. Soc. Am*. **107** 731-738
[16] Aretakis N, Mathioudakis K, Kefalakis M, et al 2004 Turbocharger unstable operation diagnosis using vibroacoustics measurements. *Trans. ASME, J. Eng. Gas Trubines Power* **126** 840-847